Article

Plasma Gas Temperature Control Performance of Metal 3D-Printed Multi-Gas Temperature-Controllable Plasma Jet

Yuma Suenaga [1], Toshihiro Takamatsu [2,3,*], Toshiki Aizawa [1], Shohei Moriya [1], Yuriko Matsumura [4], Atsuo Iwasawa [4] and Akitoshi Okino [1]

[1] Laboratory for Future Interdisciplinary Research of Science and Technology, Institute of Innovative Research, Tokyo Institute of Technology, J2-32, 4259 Nagatsuta, Midori-ku, Yokohama 226-8502, Japan; suenaga@plasma.es.titech.ac.jp (Y.S.); atoshiki@plasma.es.titech.ac.jp (T.A.); moriya@plasma.es.titech.ac.jp (S.M.); aokino@es.titech.ac.jp (A.O.)

[2] Research Institute for Biomedical Sciences, Tokyo University of Science, 2669 Yamazaki, Noda 278-0022, Japan

[3] Exploratory Oncology Research & Clinical Trial Center, National Cancer Center, 6-5-1 Kashiwanoha, Kashiwa 277-8577, Japan

[4] Division of Infection Prevention and Control, Tokyo Healthcare University, 4-1-17 Higashi-Gotanda, Shinagawa-ku, Tokyo 141-8648, Japan; y-matsumura@thcu.ac.jp (Y.M.); a-iwasawa@thcu.ac.jp (A.I.)

* Correspondence: totakama@east.ncc.go.jp

Abstract: The aim of the study was to design and build a multi-gas temperature-controllable plasma jet that can control the gas temperature of plasmas with various gas species, and evaluated its temperature control performance. In this device, a fluid at an arbitrary controlled temperature is circulated through the plasma jet body. The gas exchanges heat with the plasma jet body to control the plasma temperature. Based on this concept, a complex-shaped plasma jet with two channels in the plasma jet body, a temperature control fluid (TCF) channel, and a gas channel was designed. The temperature control performance of nitrogen gas was evaluated using computational fluid dynamics analysis, which found that the gas temperature changed proportionally to the TCF temperature. The designed plasma jet body was fabricated using metal 3D-printer technology. Using the fabricated plasma jet body, stable plasmas of argon, oxygen, carbon dioxide, and nitrogen were generated. By varying the plasma jet body temperature from $-30\,°C$ to $90\,°C$, the gas temperature was successfully controlled linearly in the range of $29–85\,°C$ for all plasma gas species. This is expected to further expand the range of applications of atmospheric low temperature plasma and to improve the plasma treatment effect.

Keywords: atmospheric plasma; metal 3D printing; temperature-controllable plasma gas

1. Introduction

Plasma has been actively applied in industrial fields, such as semiconductor manufacturing and fluorescent lighting. For example, in the field of surface treatment, plasma is used to harden the surface of materials [1] and surface modification [2]. These surface treatments are techniques that change the properties of solid surfaces using the action of the ions and electrons generated by plasma, for which low-pressure plasma has been used. Low-pressure plasmas are generated at low pressures of 1/1000 atm or less, which enables uniform surface treatment; however, this has limitations in terms of the types of treatment objects and throughput.

In recent years, it has become possible to stably generate low-temperature plasmas under atmospheric pressure; therefore, these plasmas have been applied in various fields such as medicine, industry, and chemical analysis. For example, in the medical field, they are used for disinfection [3–5], hemostasis [6], and wound healing [7], and they are used for surface modification in the industrial field [8]. In the field of chemical analysis, they have been utilized for surface adhesion analysis [9] and on-site analysis [10]. To increase

the processing effectiveness of atmospheric low-temperature plasma, the energy applied to a unit volume can be increased by means such as discharge [11]. For materials that are resistant to thermal damage, an increase in temperature promotes the reaction with the reactive species, improving the treatment effect. Ohkubo et al. reported the adhesion of PTFE using atmospheric pressure plasma controlled at 260 °C [12]. A high adhesion effect and radical density were observed in the high temperature plasma by increasing the input power. However, this temperature increase is a problem for heat-sensitive materials, such as biological samples. To solve this problem, cryo-microplasma, in which He gas is cooled by liquid nitrogen before the plasma is generated, was developed [13,14]. Oshita et al. developed a temperature-controllable atmospheric plasma source as an advanced plasma jet [15]. They succeeded in controlling the gas temperature of He plasma in the range of −54–160 °C by cooling with liquid nitrogen and heating with a heater. Another way to increase the treatment effect of atmospheric low-temperature plasma is to change the gas species of the plasma. Takamatsu et al. evaluated the effect of plasma gas species on the surface treatment effect of polyimide films and found that carbon dioxide plasma was the most effective treatment [16]. Thus, to obtain a high treatment effect without thermal damage to the target in atmospheric low-temperature plasma application, it is necessary to control the gas temperature of the plasma and generate plasmas of various gas species.

We developed a multi-gas temperature-controllable plasma jet that can easily control the gas temperature of plasmas of various gas species over a wide range of temperatures. In this study, because the temperature of gases other than He can be controlled, the excessive cooling using liquid nitrogen in the previous study must be avoided. In this study, to control the gas temperature in the plasma, the gas was stagnated in the plasma jet body before plasma generation, and heat exchange was performed. To achieve a wide temperature control range, a plasma jet body was designed and analyzed using computational fluid dynamics (CFD) to improve the temperature control performance. To fabricate a plasma jet body with a complex shape, a metal 3D printer was used. 3D-printing technology has attracted increasing attention in manufacturing, including its use in plasma systems, due to its low cost and high flexibility [17–19]. Recently, a plasma jet for an endoscope with a diameter of approximately 3 mm produced by a metal 3D printer has been reported [20]. Nitrogen, carbon dioxide, oxygen, and argon plasmas were generated using a multi-gas temperature-controllable plasma jet fabricated using a metal 3D printer. The gas temperature control performance of each plasma sample was evaluated.

2. Materials and Methods

2.1. Concept of Multi-Gas Temperature-Controllable Plasma Jet

The concept of a multi-gas temperature-controllable plasma jet is shown in Figure 1. The gas temperature before the plasma generation was controlled in the multi-gas temperature-controllable plasma jet. To achieve this, the plasma jet body was designed with a mechanism to change the gas temperature before plasma generation through heat exchange with the body. In the plasma jet body, there are two channels: a temperature control fluid (TCF) flow channel and a gas channel used to generate the plasma. The TCF flow channel spiraled around the gas channel. The plasma jet body was maintained at a constant temperature by flowing TCF through the TCF channel. The gas introduced into the plasma jet body reaches the hot and ground electrodes while conducting heat exchange with the plasma jet body. Plasma is generated by an inter-electrode discharge, and the afterglow of the plasma flows out of the plasma jet body.
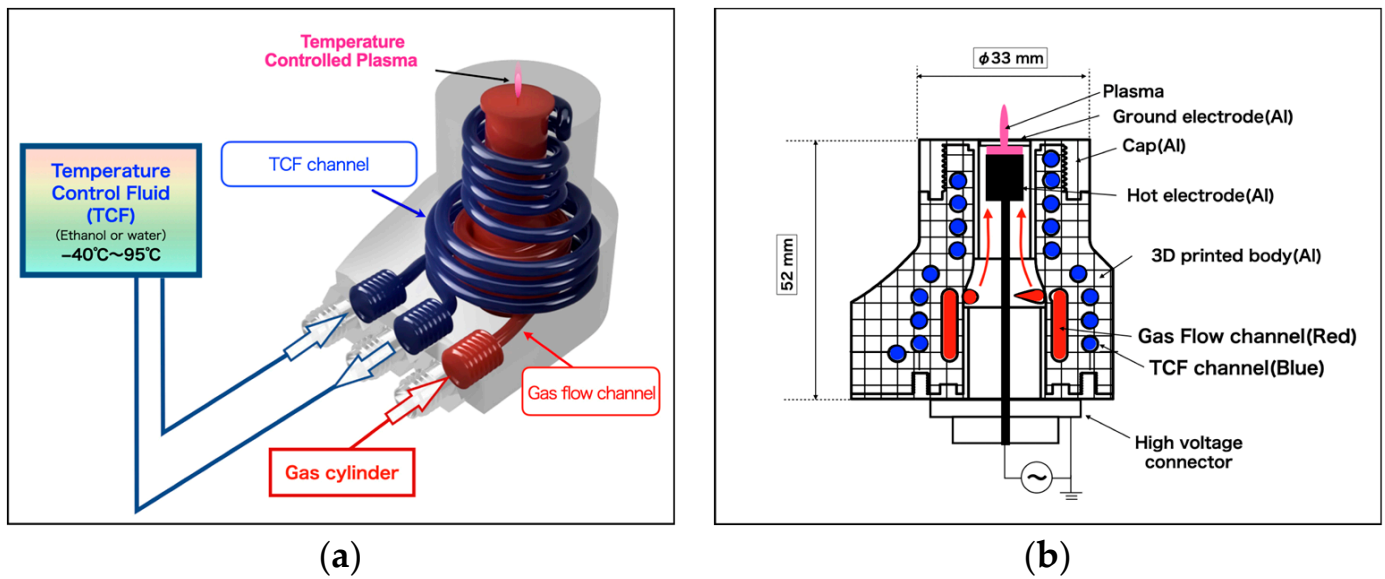
Figure 1. Concept of multi-gas temperature-controllable plasma jet: (**a**) concept of flow channel; (**b**) cross-sectional view.

2.2. Evaluation of Temperature Control Performance Using CFD Analysis

CFD analysis is used in the design of plasma devices to understand fluid dynamics and heat transfer [21]. In this study, CFD analysis using Autodesk CFD (Autodesk Inc., San Rafael, CA, USA) was performed to design the flow channels of the plasma jet. To analyze the heat transfer and gas flow, the continuity, Navier-Stokes, and energy equations are discretized and calculated by the finite element method. The respective equations for incompressible fluids are shown below. The continuity equation is

$$\rho(\nabla \cdot \boldsymbol{U}) = 0 \tag{1}$$

where ρ is the density and $\boldsymbol{U}$ is the velocity vector. The Navier-Stokes equation is

$$\rho \frac{\partial \boldsymbol{U}}{\partial t} + \rho(\nabla \cdot \boldsymbol{U})\boldsymbol{U} = \rho \boldsymbol{g} - \nabla P + \mu \nabla^2 \boldsymbol{U} \tag{2}$$

where $\boldsymbol{g}$ are the gravitational acceleration vector, P is pressure, and μ is viscosity. The energy equation is

$$\frac{\partial \rho C_p T}{\partial t} + \nabla \cdot \left(\rho C_p T \boldsymbol{U} \right) = \nabla^2 k T \tag{3}$$

where C_p is the constant pressure specific heat, T is the temperature, and k is the thermal conductivity. For turbulence analysis, these equations were time-averaged. The Reynolds stress terms generated by this averaging were approximated using the turbulence model k-ε. A modified Petrov–Galerkin method was used for calculation of the convection term in the Navier-Stokes equations. In the simplified model shown in Figure 2, the joints and screws of the parts that did not have a significant effect on the CFD were omitted. The mesh size of the model was set to "Automatic", and the parameters are resolution factor: 1.000, edge growth rate: 1.100, minimum points on edge: 2, points on longest edge: 10, surface limiting aspect: 20. The total number of nodes is 236,971 (fluid nodes: 169,458, solid nodes: 67,513), and the total number of elements is 1,008,496 (fluid elements: 532,224, solid elements: 476,272). In the analysis of the low-temperature side (-30–$0\ ^\circ$C), 80 wt% ethanol was used as the TCF and supplied to the TCF channel at a rate of 0.5 L/min. For the analysis of the high-temperature side (0–$90\ ^\circ$C), water was used as the TCF and supplied to the TCF flow channel at a rate of 0.5 L/min. The TCF was supplied to the plasma jet body using an insulated silicon rubber tube. The pressure at the outlet surface of the TCF flow channel was set to 0 Pa, and there was no pressure loss in the temperature-

controlled fluid flow. Dry nitrogen gas at 3 L/min and 24 °C was used as the gas for plasma generation. The plasma jet body was made of aluminum and surrounded by a 5 mm-thick porous ethylene propylene diene rubber insulation material. The thermal conductivity of the insulation material was set to 0.032 W/m·k. However, no insulation was placed on the surface where the plasma outlet was placed and on the upper surface because these surfaces are impediments to plasma processing in practical use. To analyze the heat transfer to the external gas, the plasma jet was placed in a nitrogen external fluid. Nitrogen at a temperature of 24 °C and humidity of 60% was used as the external fluid to match the operating environment. The surface of the external fluid was analyzed assuming no pressure loss. To clarify the effect of the temperature of the TCF on the gas before plasma generation, the temperature of the plasma jet body and gas temperature were calculated by varying the TCF from −30 to 90 °C. The temperature at the 2 mm point of the plasma outlet was calculated. A component analysis was performed on the plasma jet body, and the average temperature was calculated. It should be noted that the plasma was not considered in the CFD in this study.
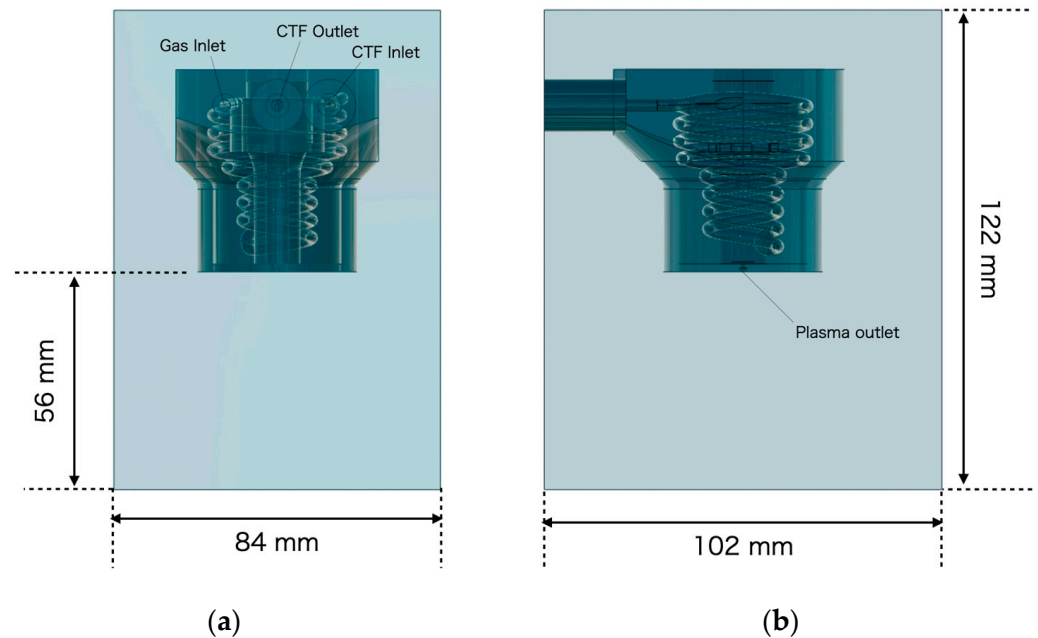
Figure 2. Geometry of multi-gas temperature-controllable plasma jet for computational fluid dynamics (CFD) analysis: (**a**) front view; (**b**) side view.

2.3. Temperature Control Performance of Multi-Gas Temperature-Controllable Plasma Jet

The temperature control performance of the multi-gas temperature-controllable plasma jet was evaluated. The designed plasma jet produced 3 L/min (standard) plasmas of carbon dioxide, argon, nitrogen, and oxygen. The plasma jet body temperature was varied from −30 to 90 °C, and the change in the plasma gas temperature was measured. For the TCF, an 80 wt% ethanol solution and water were used for the plasma jet body temperature range of −30–0 and 10–90 °C, respectively. The temperature of the TCF was controlled using a low-temperature thermostatic bath (NCB-2410B, TOKYO RIKAKIKAI CO, LTD., Tokyo, Japan) and a thermostatic bath (NCB-1210B, TOKYO RIKAKIKAI CO, LTD., Tokyo, Japan) at −30–0 °C and 10–90 °C, respectively.

The temperature of the plasma jet body was measured using a K-type thermocouple attached to the side of the body and a logger (RX-450K, AS ONE CORPORATION, Osaka, Japan). The TCF temperature was measured using a K-type thermocouple in the TCF channel immediately before the plasma jet body. The plasma gas temperature was measured using a K-type thermocouple at a distance of 2 mm from the plasma outlet 120 s after the plasma was generated. The temperature at each gas irradiation without the

plasma generation was also measured under the same conditions. The ambient temperature and humidity were 22 °C and 60%, respectively. The plasma jet body was covered with insulation material to reduce the influence of the surrounding environment.

3. Results and Discussion

3.1. Evaluation of Temperature Control Performance Using CFD Analysis

CFD analysis was performed to design the flow path of the multi-gas temperature-controllable plasma jet. Figure 3a,b show the temperature distribution in the cross-section of the plasma jet when a TCF of −30 °C and 90 °C flows in the TCF channel, respectively. When a TCF of −30 °C was supplied, the average temperature of the plasma jet body decreased to −29.1 °C. The gas temperature 2 mm from the plasma outlet was −23.0 °C. When a TCF of 90 °C was supplied, the temperature of the plasma body was 89.5 °C. The gas temperature at 2 mm from the plasma outlet was 82.1 °C. In each case, it was shown that the gas temperature approached the room temperature of 24 °C as the distance from the plasma outlet increased.


(**a**)　　　　　　　　　　　　　　(**b**)

(**c**)
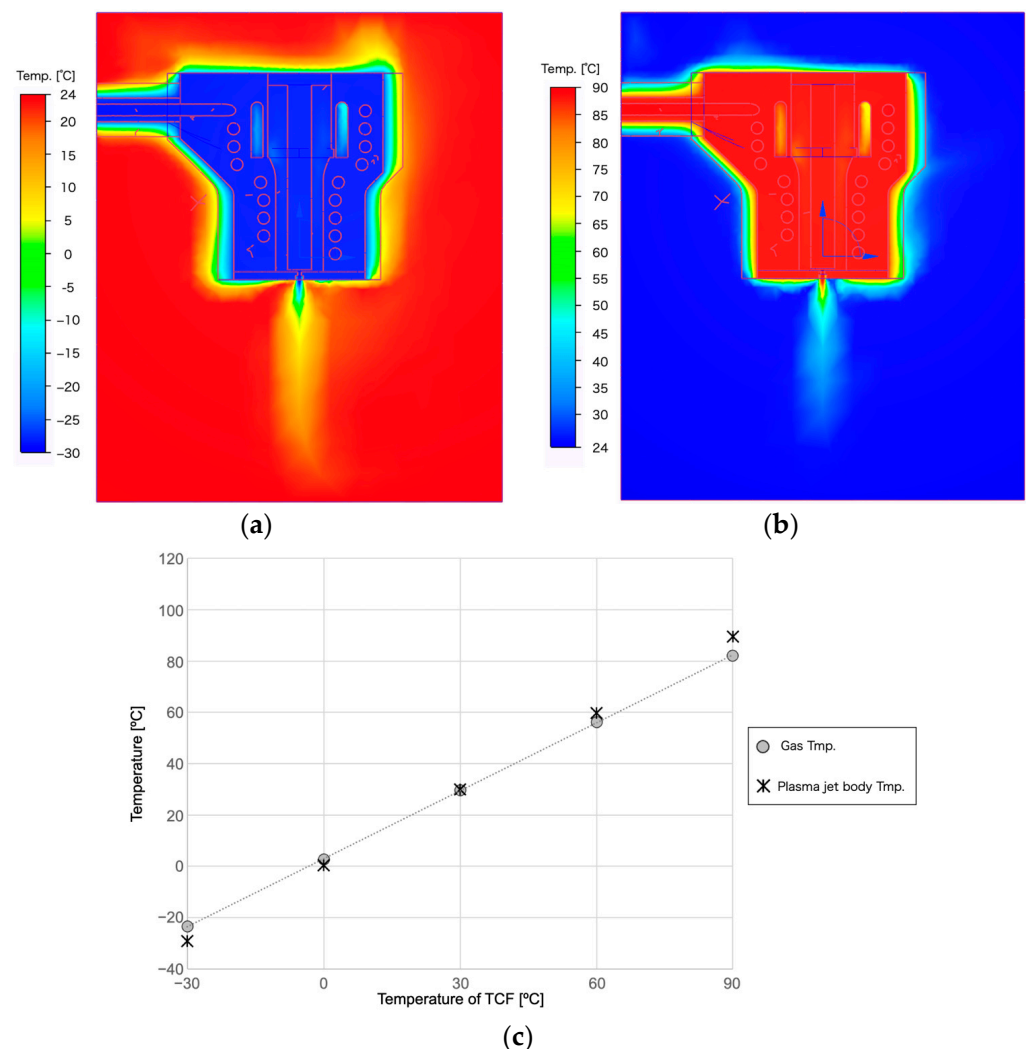
Figure 3. Evaluation of plasma jet body using CFD analysis: (**a**) temperature distribution at temperature control fluid (TCF) of −30 °C; (**b**) temperature distribution at TCF of 90 °C; (**c**) gas temperature at a distance of 2 mm from the plasma outlet calculated by CFD.

Figure 3c shows the relationship between the TCF temperature and gas temperature at a distance of 2 mm from the plasma outlet. As the TCF temperature increased, the gas temperature increased proportionally. The CFD analysis shows that the gas temperature

before the plasma generation can be easily changed using a plasma jet body containing a TCF channel. It has been reported that the gas temperature of the plasma can be changed by varying the gas temperature before the plasma generation [15]. The gas temperature of the plasma can also be controlled by varying the TCF temperature used in the designed plasma jet.

3.2. Fabrication of Multi-Gas Temperature-Controllable Plasma Jet

The CFD analysis showed that the gas temperature could be controlled by the TCF temperature. Therefore, a multi-gas temperature-controllable plasma jet containing a TCF channel and a gas channel was fabricated. This device is difficult to fabricate by general machining due to the complex flow channels inside the plasma jet body. The plasma jet body was fabricated using a direct metal-printing 3D printer (Prox300 from 3DSystems Inc., San Diego, CA, USA) that sintered the metal powder with a laser. The plasma jet body was fabricated by SOLIZE Corporation, Tokyo, Japan. The metal powder used was aluminum–silicon alloy (AlSi12), which has excellent thermal conductivity. In the particle size distribution of metal powder, D10, D50, D90 were 9 µm, 20 µm, and 36 µm, respectively. When the metal powder is reused, it is sieved to remove foreign matter. The parameters of the 3D printer are 40 µm thickness per layer. The standard tolerance of the built object is ±0.3 mm. The parts that required high precision, such as screws and parts that needed to be airtight, were fabricated using machine tools. The fabricated plasma jet is shown in Figure 4a. The plasma was generated by applying a sinusoidal wave of 9 kV and 16 kHz to the hot electrode of the fabricated plasma jet. Figure 4b shows the generated plasmas of carbon dioxide, argon, nitrogen, and oxygen. Stable plasma generation was observed in the plasma jet body with multiple channels formed by a metal 3D printer.
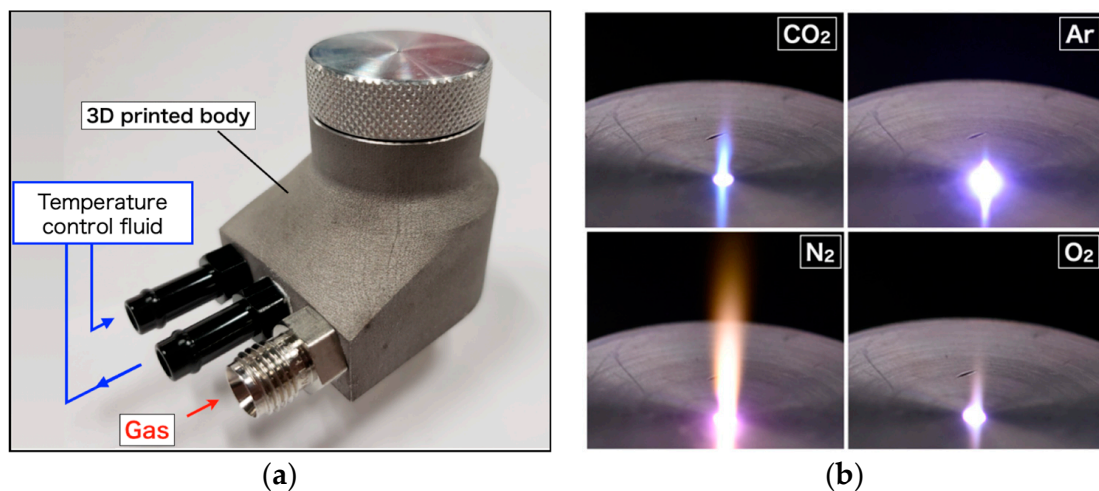

Figure 4. Metal 3D-printed multi-gas temperature-controllable plasma jet: (**a**) outside view; (**b**) plasma generation for various gas species.

3.3. Temperature Control Performance of Multi-Gas Temperature-Controllable Plasma Jet

Figure 5 shows the relationship between the TCF temperature, the plasma jet body temperature, and the gas temperature before and after the plasma generation. The results of the CFD analysis are also plotted in the N_2 result. The gas and plasma gas temperatures of carbon dioxide, argon, nitrogen, and oxygen were varied in the ranges of −17–77 and 29–108, −18–74.5 and 3–85, −20–78 and 28–108, and −21–78 and 17–106 °C, respectively, by varying the plasma jet body temperature from −30 °C to 90 °C. Assuming that the plasma jet body temperature affects the plasma gas temperature, a single regression analysis was performed. The coefficients of determination for each approximation line are listed in Table 1. In the case of gas irradiation, the coefficients of determination for the R^2 values were greater than 0.99 for all gas species. The gas temperatures of the plasmas had a

coefficient of determination for the R^2 values greater than 0.98 for all gas species. These results show that the approximation line fits effectively and that the plasma jet body temperature, gas temperature, and plasma gas temperature vary proportionally. The gas temperature of the plasma was indirectly controlled by controlling the temperature of the plasma jet body. The instability of the plasma gas temperature was observed when the plasma jet body temperature was between −10 °C and 20 °C because of the water droplets that condensed on the plasma jet body near the plasma outlet. These water droplets were caught in the gas flow of the plasma, causing instability in the plasma temperature. When the measured nitrogen gas temperature was compared with the CFD temperature control performance, a decrease in the temperature control performance of approximately 3 °C and 5 °C was observed at a plasma jet body temperature of −30 and 90 °C, respectively. The CFD results and actual measurements were not in perfect agreement. This may be due to the fact that the CFD does not reproduce external disturbances such as the air flow around the plasma jet.
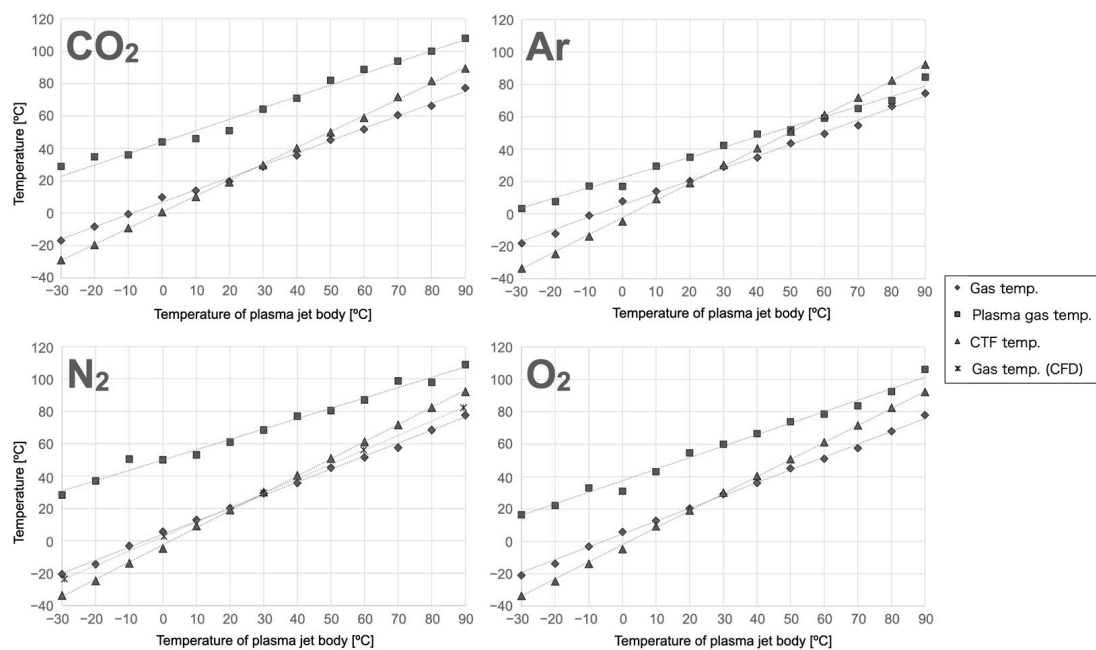
Figure 5. Relationship between plasma gas temperature and plasma jet body temperature.

Table 1. Coefficient of determination between plasma jet body temperature and gas temperature for each gas species.

	CO_2	Ar	N_2	O_2
Gas	0.9975	0.9967	0.9981	0.9996
Plasma	0.9828	0.9898	0.9861	0.9893

For all gas species, a temperature increase was observed when the plasma was generated. The ranges of the temperature increase for carbon dioxide, argon, nitrogen, and oxygen at the plasma jet body temperature of −30 °C were 46, 22, 49, and 37 °C, respectively. The range of temperature increase for carbon dioxide, argon, nitrogen, and oxygen at the plasma jet body temperature of 20 °C, which was close to the room temperature, was 31, 15, 41, and 34 °C, respectively. The temperature increase for carbon dioxide, argon, nitrogen, and oxygen at the plasma jet body temperature of 90 °C was 31, 10, 31, and 28 °C, respectively. For all gas species of plasma, the range of temperature increase due to plasma generation decreased as the gas temperature increased. One of the reasons for this phenomenon may be the influence of the room temperature through mixing with the

ambient air. To achieve lower or higher plasma gas temperatures, it is necessary to vary the temperature of the TCF significantly.

By lowering the temperature of the plasma jet body to -30 °C, a plasma gas temperature of less than 30 °C can be achieved, and irradiation of heat-sensitive processing materials such as plants is possible. Gas temperatures up to 108 °C can be achieved in carbon dioxide and nitrogen plasmas, which is useful for studying the conditions for improving the treatment effect. In the future, the developed multi-gas temperature-controllable plasma jet will be applied in medical and agriculture applications. Additionally, it is necessary to clarify the gas species and gas temperature of the plasma to maximize the treatment effect.

4. Conclusions

In this study, we developed a multi-gas temperature-controllable plasma jet that can generate plasma of various gas species at an arbitrary controlled temperature. A multi-gas temperature-controllable plasma jet was designed using CFD analysis with a TCF channel spiraled around the gas channel. The designed plasma jet was fabricated using metal 3D-printer technology. In the multi-gas temperature-controllable plasma jet, the stable generation of the plasma of nitrogen, oxygen, carbon dioxide, and argon was successfully achieved. The temperature of the plasma gas can be easily changed by controlling the temperature of the supplied TCF. Additionally, the gas temperature after plasma generation changed linearly by changing the TCF temperature. The gas temperature of the plasma was controlled between a minimum of 3 °C and a maximum of 108 °C by varying the plasma jet body temperature from -30 to 90 °C. The gas temperature was increased by the plasma generation. The range of the temperature increase obtained for carbon dioxide, argon, nitrogen, and oxygen was 31, 15, 41, and 34 °C, respectively, when the plasma jet body temperature was 20 °C. These results indicate that the gas temperature control characteristics of plasma vary significantly depending on the gas species.

It was shown that it is possible to design and fabricate plasma jets with a higher level of flexibility. A multi-gas temperature-controllable plasma jet of any shape can be fabricated for plasma applications in medicine, agriculture, and material processing. The use of multi-gas temperature-controllable plasma jets is expected to control the gas temperature of the plasma of various gas species and achieve stable treatment effects without damaging the treated object. In the future, we will study the gas species and temperature of the plasma for various applications such as hemostasis, disinfection, surface treatment, and plant genome editing.

References

1. Kashapov, N.F.; Sharifullin, S.N. Hardening of the Surface Plasma Jet High- Frequency Induction Discharge of Low Pressure. *Mater. Sci. Eng. Pap.* **2015**, *86*, 012021. [CrossRef]
2. Wilson, D.J.; Williams, R.L.; Pond, R.C. Plasma Modification of PTFE Surfaces. *Surf. Interface Anal.* **2001**, *31*, 385–396. [CrossRef]
3. Pan, J.; Li, Y.L.; Liu, C.M.; Tian, Y.; Yu, S.; Wang, K.L.; Zhang, J.; Fang, J. Investigation of cold atmospheric plasma-activated water for the dental unit waterline system contamination and safety evaluation in vitro. *Plasma Chem. Plasma Process.* **2017**, *37*, 1091–1103. [CrossRef]
4. Maisch, T.; Shimizu, T.; Li, Y.F.; Heinlin, J.; Karrer, S.; Morfill, G.; Zimmermann, J.L. Decolonisation of MRSA, *S. Aureus* and *E. Coli* by Cold-Atmospheric Plasma Using a Porcine Skin Model In Vitro. *PLoS ONE* **2012**, *7*, e34610. [CrossRef]
5. Abonti, T.R.; Kaku, M.; Kojima, S.; Sumi, H.; Kojima, S.; Yamamoto, T.; Yashima, Y.; Miyahara, H.; Okino, A.; Kawata, T.; et al. Irradiation Effects of Low Temperature Multi Gas Plasma Jet on Oral Bacteria. *Dent. Mater. J.* **2016**, *35*, 822–828. [CrossRef] [PubMed]
6. Fridman, G.; Peddinghaus, M.; Ayan, H.; Fridman, A.; Balasubramanian, M.; Gutsol, A.; Brooks, A.; Friedman, G. Blood Coagulation and Living Tissue Sterilization by Floating-Electrode Dielectric Barrier Discharge in Air. *Plasma Chem. Plasma Process.* **2006**, *26*, 425–442. [CrossRef]
7. Shimatani, A.; Toyoda, H.; Orita, K.; Hirakawa, Y.; Aoki, K.; Oh, J.; Shirafuji, T.; Nakamura, H. In Vivo Study on the Healing of Bone Defect Treated with Non-Thermal Atmospheric Pressure Gas Discharge Plasma. *PLoS ONE* **2021**, *16*, e0255861. [CrossRef]
8. Černáková, L.; Kováčik, D.; Zahoranová, A.; Černák, M.; Mazúr, M. Surface Modification of Polypropylene Non-Woven Fabrics by Atmospheric-Pressure Plasma Activation Followed by Acrylic Acid Grafting. *Plasma Chem. Plasma Process.* **2005**, *25*, 427–437. [CrossRef]
9. Aida, M.; Iwai, T.; Okamoto, Y.; Kohno, S.; Kakegawa, K.; Miyahara, H.; Seto, Y.; Okino, A. Development of a Dual Plasma Desorption/Ionization System for the Noncontact and Highly Sensitive Analysis of Surface Adhesive Compounds. *Mass Spectrom.* **2017**, *6*, S0075. [CrossRef] [PubMed]
10. Iwai, T.; Kakegawa, K.; Aida, M.; Nagashima, H.; Nagoya, T.; Kanamori-kataoka, M.; Miyahara, H.; Seto, Y.; Okino, A. Development of a Gas-Cylinder-Free Plasma Desorption/Ionization System for On-Site Detection of Chemical Warfare Agents. *Anal. Chem.* **2015**, *87*, 5707–5715. [CrossRef] [PubMed]
11. Van Deynse, A.; Cools, P.; Leys, C.; De Geyter, N.; Morent, R. Surface Activation of Polyethylene with an Argon Atmospheric Pressure Plasma Jet: Influence of Applied Power and Flow Rate. *Appl. Surf. Sci.* **2015**, *328*, 269–278. [CrossRef]
12. Ohkubo, Y.; Ishihara, K.; Shibahara, M.; Nagatani, A.; Honda, K.; Endo, K.; Yamamura, K. Drastic Improvement in Adhesion Property of Polytetrafluoroethylene (PTFE) via Heat-Assisted Plasma Treatment Using a Heater. *Sci. Rep.* **2017**, *7*, 9476. [CrossRef] [PubMed]
13. Noma, Y.; Choi, J.H.; Tomai, T.; Terashima, K. Gas-Temperature-Dependent Generation of Cryoplasma Jet under Atmospheric Pressure. *Appl. Phys. Lett.* **2008**, *93*, 101503. [CrossRef]
14. Ishihara, D.; Noma, Y.; Stauss, S.; Sai, M.; Tomai, T.; Terashima, K. Development of a Dielectric Barrier Discharge (DBD) Cryo-Microplasma: Generation and diagnostics. *Plasma Sources Sci. Technol. Dev.* **2008**, *17*, 035008. [CrossRef]
15. Oshita, T.; Kawano, H.; Takamatsu, T.; Miyahara, H.; Okino, A. Temperature Controllable Atmospheric Plasma Source. *IEEE Trans. Plasma Sci.* **2015**, *43*, 1987–1992. [CrossRef]
16. Takamatsu, T.; Hirai, H.; Sasaki, R.; Miyahara, H.; Okino, A. Surface Hydrophilization of Polyimide Films Using Atmospheric Damage-Free Multigas Plasma Jet Source. *Kagaku Kogaku Ronbunshu* **2013**, *39*, 372–377. [CrossRef]
17. Martínez-Jarquín, S.; Moreno-Pedraza, A.; Guillén-Alonso, H.; Winkler, R. Template for 3D Printing a Low-Temperature Plasma Probe. *Anal. Chem.* **2016**, *88*, 6976–6980. [CrossRef] [PubMed]
18. Barillas, L.; Makhneva, E.; An, S.; Fricke, K. Functional Thin Films Synthesized from Liquid Precursors by Combining Mist Chambers and Atmospheric-Pressure Plasma Polymerization. *Coatings* **2021**, *11*, 1336. [CrossRef]
19. Takamatsu, T.; Kawano, H.; Miyahara, H.; Azuma, T.; Okino, A. Atmospheric Nonequilibrium Mini-Plasma Jet Created by a 3D Printer. *AIP Adv.* **2015**, *5*, 077184. [CrossRef]
20. Kurosawa, M.; Takamatsu, T.; Kawano, H.; Hayashi, Y.; Miyahara, H.; Ota, S.; Okino, A.; Yoshida, M. Endoscopic Hemostasis in Porcine Gastrointestinal Tract Using CO_2 Low-Temperature Plasma Jet. *J. Surg. Res.* **2018**, *234*, 334–342. [CrossRef] [PubMed]
21. Onyshchenko, I.; De Geyter, N.; Morent, R. Improvement of the Plasma Treatment Effect on PET with a Newly Designed Atmospheric Pressure Plasma Jet. *Plasma Process. Polym.* **2017**, *14*, 1600200. [CrossRef]